Appendix 1

Single channel patch clamping: achieving a high temporal resolution and a low noise

George Shapovalov

Index

Sources of noise

Major sources of noise in the electrical signal during patch clamping classically are considered to be localized to the recording area and include: 1) thermal and 2) shot noise produced by the patch of the membrane, 3) intrinsic noise in the pipette and pipette holder, and 4) noise of the current-to-voltage converter. Below I discuss these sources of noise in detail.

Spectral density of the noise for the system in thermal equilibrium, whose equivalent circuit can be constructed of passive elements, in general is given by (Gupta, 1977)

$$S^2(f) = 4kT\ \mathrm{Re}\{Y(f)\} \qquad (1)$$

where *Y(f)* is the patch admittance that in general depends on frequency *f*.

1) In the case of Johnson noise and a representation of a membrane patch as a simple parallel RC circuit we have, for current noise, Re *Y(f) = 1/R* or power spectrum density of *4kT/R*. Apparently this source of noise can be minimized by increasing the resistance of the patch (the gigaseal resistance). The patch resistance is influenced by the pipette glass and internal diameter; however it primarily depends on the skill of the experimenter.

2) Shot noise, or counting noise, arises when charge carriers cross a potential barrier, the situation almost universally taking place in ion conduction events. Power spectrum density of shot noise is given by (Gupta, 1977)

$S^2 = 2Iq$,

where q is the charge of current carrier (for unit charge $q = 1.6 \times 10^{-19}$ C) and I is the amplitude of the measured current through the patch. Therefore, ion channels of higher electrical conductance provide the advantage that a higher number of electrical carriers taking part in single conduction events and thus higher signal-to-noise ratio. Additionally, optimizing the salt concentrations of the recording solutions or increasing the voltage applied across the membrane allows one to maximize overall current

and thus to obtain higher signal-to-noise ratios.

3) Intrinsic noise in the pipette has three major sources: a thin layer of solution creeping up the pipette, bulk conductivity of the pipette, and a combination of the pipette access resistance and the tip capacitance. All of these sources can be represented as a series RC circuit with noise spectral density given by

$$\mathrm{Re}\{Y(f)\} = \frac{(\omega RC)^2}{R(1+(\omega RC)^2)}, \qquad (2)$$

where $\omega = 2\pi f$. In the high-frequency limit this approaches 1/R and at low frequencies this formula can be simplified to $\mathrm{Re}\{Y(f)\} = (\omega C)^2 R$, which increases quadratically with frequency.

Typically, the largest of these three noise sources is a thin layer of solution on the outside of the pipette. A thin film forms a conductive layer with a distributed resistance on the order of 100 MΩ (Hamill et al., 1981) which is coupled to the solution inside the pipette over a distributed wall capacitance of a few pF. In the high-frequency approximation this corresponds roughly to the thermal noise of 100 MΩ resistor, a couple of orders of magnitude larger than that produced by the patch itself. Fortunately the formation of solution layer can be decreased by applying Sylgard coating to the external surface of the pipette (Hamill et al., 1981; Benndorf, 1995). The hydrophobic surface of the Sylgard coating prevents formation of a thin solution film, and extra thickness added by the coating reduces pipette capacitance. Even stronger reduction of noise can be achieved by using thick-wall quartz pipettes (Levis and Rae, 1993; Parzefall et al., 1998). The advantages include hydrophobicity and good dielectric properties of quartz glass and avoidance of the possibility that the solution could leak beneath the layer of Sylgard (J. Dudel, personal communication). The only serious disadvantage of quartz pipettes is a requirement to use special pipette pullers, such as CO_2-laser based Sutter Instruments P2000 or H-O based pullers (Dudel et al., 2000).

Dielectric properties of the pipette can play a significant role as well. Bulk conductivity of the softer

types of glass can be significant, especially at frequencies above 1 kHz (1993). Applying Sylgard coating decreases the dielectric loss, however in this case it is also advantageous to use quartz pipettes with high outer to inner diameter ratio.

Pipette access resistance (typically 2-5 MΩ) and tip capacitance (typically 0.2-0.4 pF) form a series RC connection with a time constant $\leq$ 1 μs. In the low-frequency regime (< ~500 kHz) this source of noise behaves proportionally to $(\omega C)^2 R$ and thus can be decreased by making R and C smaller. Both of these parameters depend mostly on the geometry of the pipette. It is therefore advantageous to achieve a steeper tip angle and to use thick walled glass with high outer to inner diameter ratio or, if a coating is used, to extend it closer to the tip of the pipette.

Lastly, bulk conductivity of the material and the shape, are also important for the pipette holder. Teflon or polycarbonate can be used as the material for the pipette holder (Levis and Rae, 1993), it is also advisable to avoid metal shields on the pipette holder, as that significantly increases its capacitance. However an even better approach is to eliminate the pipette holder altogether, leaving only the gasket mounted directly to the modified outlet of the headstage, as was performed in (Parzefall et al., 1998). Figure 1 shows the CV 203BU headstage (Axon Instruments) modified mechanically during the author's visit to the J. Dudel group (Institut für Physiologie der Technischen Universität München, Biedersteiner Strasse 29, D-80802 Munich, Germany). The modification involved removing the universal Teflon connector used by Axon Instruments in all recent models and replacing it with a small Teflon ring with a radial inset in the center, designed to hold a Sylgard gasket pressurizing the pipette. A hole was drilled on the side of the Teflon ring (and trough one of the metal plates protecting the headstage) and a metal tube (with the diameter of ~1 mm) was installed to serve as a pressure inlet. The pipette is held by the metal V-shaped lever and nut assembly attached (mechanically and electrically) to the metal headstage enclosing. A spring-loaded lever was used to press against the Sylgard gasket thus pressurizing the holder before suction application, as shown on Figure 1.

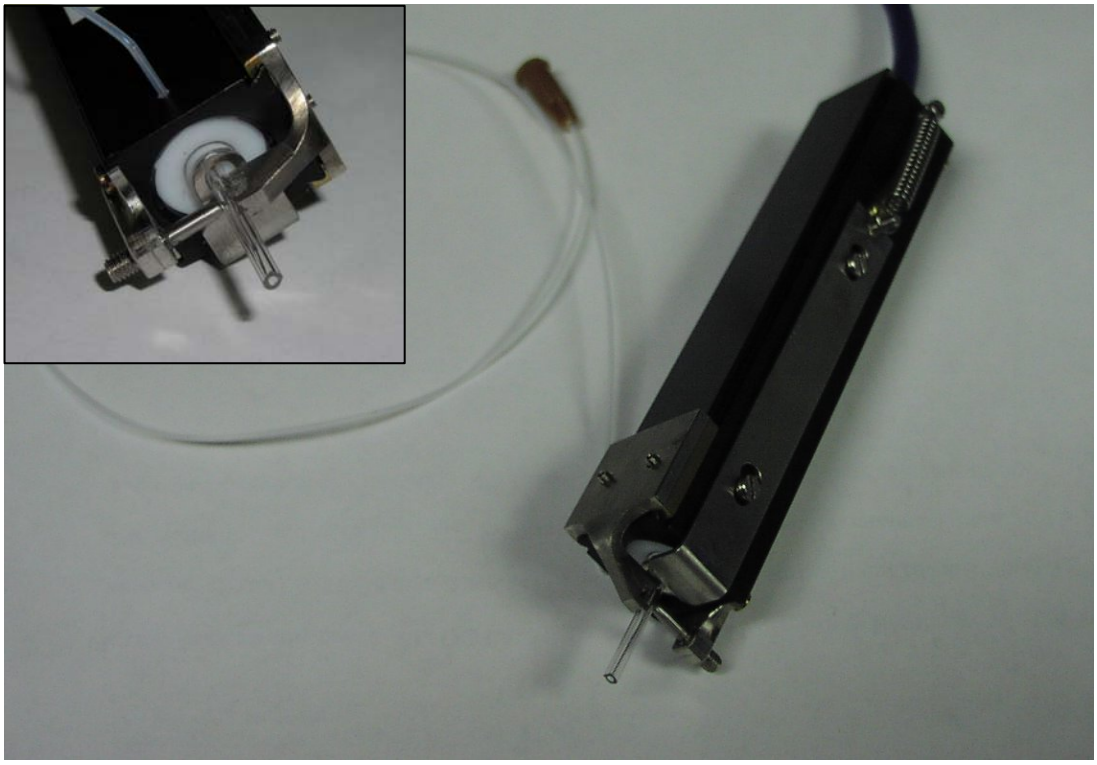

Figure 1. The headstage (CV 203BU, Axon Instruments) modified for low noise single channel data acquisition. The universal Teflon connector used by Axon Instruments is replaced by metal pipette mounts and a removable Sylgard gasket. The inset shows a close-up view of the pipette mount.

4) Noise in the current-to-voltage converter. Schema 1 shows the principal electric scheme of the headstage electronics involved in the processing of the signal. The headstage can operate in resistive (R-) or capacitive (C-) feedback modes.

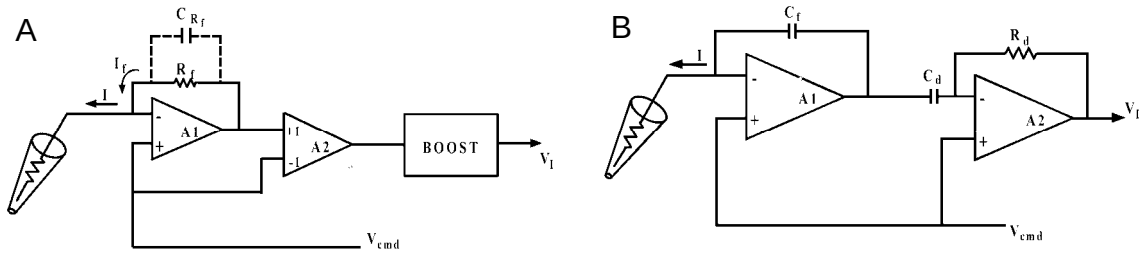

Schema 1. Principal electric scheme of a first cascade of amplification of a CV 203BU headstage in resistive (A) and capacitive (B) feedback modes. (A) Differential amplifier A2 subtracts V_{cmd} from the output of A1 which makes the output proportional to the voltage across R_f and thus measured current. Boost circuitry increases the gain at high frequencies to compensate for the narrow bandwidth of a feedback resistor. (B) The output of the amplifier A1 is proportional to the integral of the pipette current. The actual current is recovered by differentiating it via the differentiator formed by the C_d, R_d and A2 assembly.

In the R-feedback mode the predominant source of noise is a thermal noise in the feedback resistor R_f. In order to decrease the noise it is essential to use high values of R_f; values in the range of 10-50 GΩ are typical in low noise amplifiers. Such high gigohm resistors are hard to produce and often exhibit noise exceeding that predicted by the simple *1/R* relationship. Moreover, a high value of feedback resistance limits maximum level of current that can be passed by the circuitry (typically 200 pA for a 50 GΩ R_f) and has an adverse effect on the effective bandwidth (discussed below). For these reasons C-feedback mode is commonly used in low-noise electrophysiology measurements.

Use of a capacitance as a feedback element decreases thermal noise and increases bandwidth as well as dynamic range of the amplifier. Capacitors do not generate so much thermal noise as resistors (thermal noise of an ideal capacitor is zero). However, since C_f effectively sums with the other sources of input capacitance, in order to take full advantage of the benefits it is necessary that C_f does not exceed the stray capacitance of the pipette/headstage assembly (typically on an order of 10 pF) which, ideally, should also be minimized.

The sources described here are well characterized and usually play a major role during single-channel recordings at moderate bandwidths of 1 - 50 kHz. However, according to the author's experience, electrical interference starts to dominate at frequencies > 100 kHz. Additionally, it was found that at such frequencies the length and quality of coaxial cables connecting the instruments play an important role in avoiding adding distortions and excess noise to the measured signal.

Minimizing electrical interference

A typical electrophysiology setup combines a multitude of components that must work in tight accord in order to produce clean and reliable data. Major components employed in a typical setup

include an inverted microscope (the author used Leitz Diavert with 40x phase-contrast objective, NA 0.55), micromanipulators (Burleigh, PCS-5000), a chamber with a sample and a solution exchange system, a pipette and amplifier headstage assembly, an amplifier (Axopatch 200B, Axon Instruments), a digitizer (Digidata 1322A) and a computer. All but the last three of the listed components form a tight assembly in immediate vicinity of the sample, thus creating a significant bulk of metal and dielectric parts. It is therefore important to optimize the physical layout of the components of the electrophysiological setup in order (a) to minimize electrical interference and stray capacitance introduced by the components and (b) to provide adequate grounding and shielding.

Schema 2 presents the layout adapted by the author. Dotted lines represent shielding enclosures, an external Faraday cage containing vibration isolation table, amplifier and the microscope, micromanipulator and recording chamber assembly as well as secondary shield isolating the headstage with the pipette and the sample. In order to decrease EM penetration we used an Al garden shed (House of Redwood) as a Faraday cage. The shed was scraped at joints to remove the paint and the sheets were tightly overlaid at joints in order to avoid any openings. The shed was additionally fitted with an Al floor to reduce EM interference through the concrete floor of the building. The shed and the vibration isolation table were connected to the ground return at the back of the amplifier with care taken not to create ground loops.

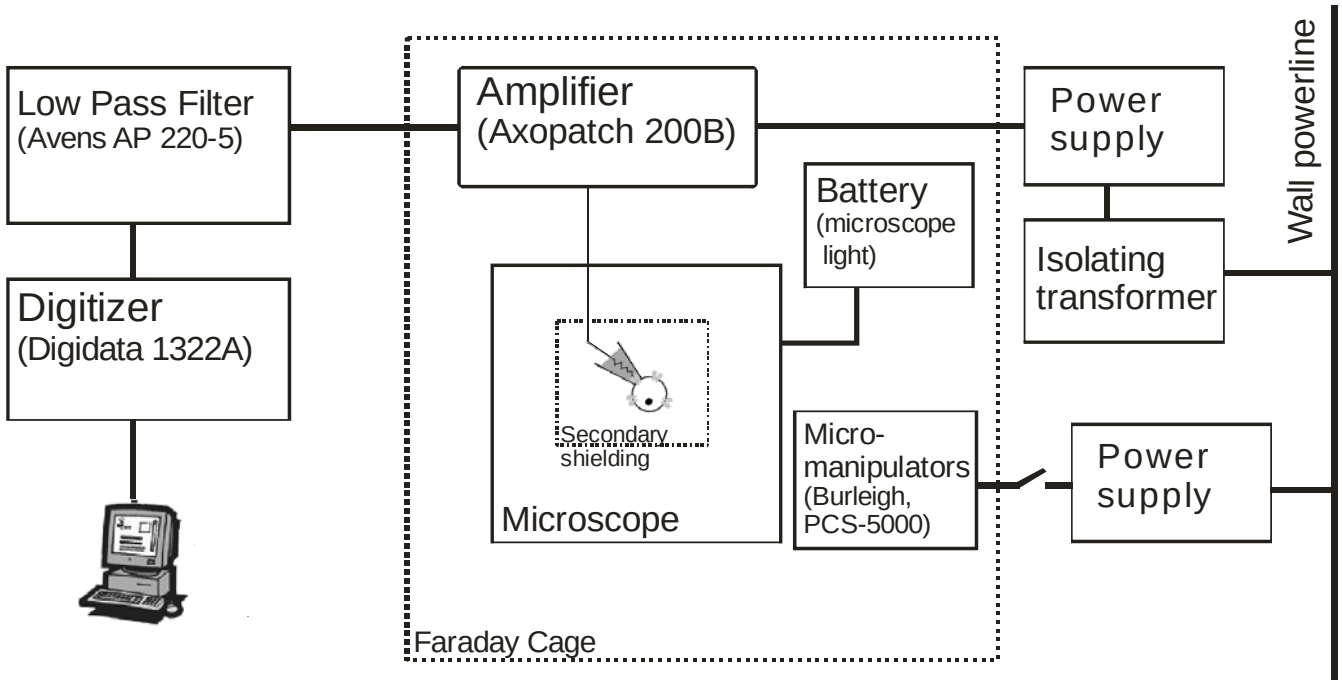

Schema 2 Principal scheme presenting the components of a single-channel patch clamp setup and their interconnections. The layout emphasizes the steps taken by the author to group the components in order to provide appropriate shielding and decrease electrical interference. Dotted rectangles represent two layers of shielding: the Al garden shed used as a Faraday cage and a secondary layer of shielding made of Al foil in near vicinity of a recording chamber.

The only electronic components positioned inside the shed were the amplifier, micromanipulators and headstage assembly and a microscope light. The power supply for the micromanipulators was outside the shed. In addition a switch was installed that allowed to disconnect the micromanipulators from the power supply and to connect the assembly residing inside the shed to the common ground return of the amplifier. This significantly decreased the apparent interference introduced via the connection feeding the micromanipulators when the switch was flipped to the "grounded" position after the gigaseal formation and during the actual data acquisition. The microscope light (6 V, 15 W bulb) was powered from a 12 volt car battery (Prostart, 165 amp-hours). The power supplied to the microscope light was regulated with a 3 Ω rheostat (Ohmite, maximum current of 5 amperes). The power supply of the Axopatch amplifier was removed and placed in a separate enclosure outside of the shed. In general, care was taken to ensure that only DC power was entering the shed and the only active

connection during the data acquisition phase was that from the amplifier to the digitizer. Additionally the area inside the shed was cleaned so as to remove all unnecessary metal or dielectric parts. Figure 2 shows the inside view of the shed after the assembly.

Figure 2. View of the single-channel patch clamp assembly optimized for high time resolution and low noise. Attention was paid to keep only necessary components inside the Faraday cage and to minimize the number of electrical connections entering the cage.

Secondary shielding protecting the headstage and the recording chamber was provided by the aluminum foil (Reynolds wrap, .045 in) that was connected to the ground return at the back of the headstage. In order to minimize stray capacitance added by the secondary shield, the foil was kept on average 10 cm away from the pipette, approaching within ~ 1 cm near the recording chamber. In order to reduce the interference carried over power lines, the amplifier power supply was connected to the wall power line through an isolating transformer (0211T35ST; Topaz Electronics).

At frequencies above 200 kHz, additional interference was produced by the amplifier itself. The Axopatch 200B, as shipped by the supplier, was tuned for maximum suppression of capacitive reset transients. However in such mode it produced an interference pattern that had a characteristic

frequency ramping from 500 kHz down to 300 kHz. This interference pattern clearly correlated to the accumulated charge on the feedback capacitor. To reduce the impact of this interference source, the compensation circuitry was tuned for a suitable compromise between compensation of reset transients and diminished interference by the reset circuitry.

Increasing the bandwidth

The measures described above allowed an improved signal-to-noise ratio, thus making it possible to capture higher signal frequencies. The Axopatch 200B amplifier, while having a bandwidth and noise characteristics among the best of the commercially available amplifiers, is still limited to 100 kHz. Further I describe the modifications that allow extended acquisition bandwidth.

As mentioned above, the amplifier can operate in resistive and capacitive feedback modes. The use of resistive feedback mode, in addition to higher noise, has and added disadvantage of a limited bandwidth. Typical values of R_f = 50 GΩ and $C_{R_f} = 0.1\,\text{pF}$ give a time constant of 5 ms, emphasizing the need for additional circuitry boosting amplifier gain at higher frequencies. However representation of R_f as a parallel combination of ideal resistor and capacitor is only approximate, which necessitates the use of considerably more complex boosting circuitry in the amplifier (Axon Guide). Moreover, even a four-pole/three-zero boosting circuit does not provide a perfect correction of the frequency response of R_f. Due to imperfect compensation, the response to square pulse occasionally showed overshoots as large as 2% of total amplitude (Axon Guide). Use of a capacitance as a feedback element avoids formation of an effective low-pass RC filter at the first stage of amplification. Another consequence of using C-feedback mode of the headstage is that the output voltage of A1 amplifier on Schema 1B becomes proportional to the accumulated charge rather than the current. A differentiating cascade is then used to recover the actual current.

Frequency response of a headstage in C-feedback can be characterized by an equivalent transfer resistance

$$R_T = R_d \frac{C_d}{C_f}$$

In the case of an ideal feedback capacitor, noise is independent of C_f, thus R_T can be kept quite low, in sub GΩ range. This greatly increases effective amplifier bandwidth as well as maximum current that can be passed through a headstage, resulting in increased dynamic range.

Use of a capacitance as a feedback element has a disadvantage: in the presence of a net DC current in measured signal, C_f accumulates charge which eventually leads to overload of operational amplifier A1. This necessitates circuitry periodically resetting the capacitor charge to zero. For C_f = 1 pF in the case of the CV 203BU headstage, 1 nA net current and Axopatch 200B circuitry operating in the range of ±10 V the resets need to be performed every 10 ms. The duration of the reset is approximately 50 μs (Axon Guide, p 95) which leads to the loss of ~0.5% of the data under such conditions.

As shipped by supplier the Axopatch 200B amplifier is calibrated to allow low-noise data acquisition at frequencies up to 100 kHz. Achieving higher bandwidth requires additional modifications, as described below. The modifications to the amplifying stages were suggested by Richard Lobdill (Axon Instruments) and were performed locally by the authors. The modifications can be classified in two principal steps

- Reducing the gain of the digitizer 10-fold, thus reducing the transfer resistance of the headstage in C-feedback mode. Necessary modifications are:

    1. Change R3 from 150 kΩ to 15 kΩ.

    2. Change C17 from 10 pF to 47 pF.

    Decreasing digitizer gain further did not yield additional improvement to the bandwidth (R. Lobdill, personal communication).

- Bypassing the 10 kHz low-pass filter that leads to the I_{out} output at the back of the amplifier. The necessary steps are:

    1. Remove C140.
    2. Short out C240.
    3. Remove R13 and R225.
    4. Connect Pin 1 of U95 (the connection of the removed R225 may be used for contact) to the rear panel BNC marked I_{out} (again, the connection of removed R13 may be used for contact).

The modifications are summarized in Schema 3 and

Figure 3.

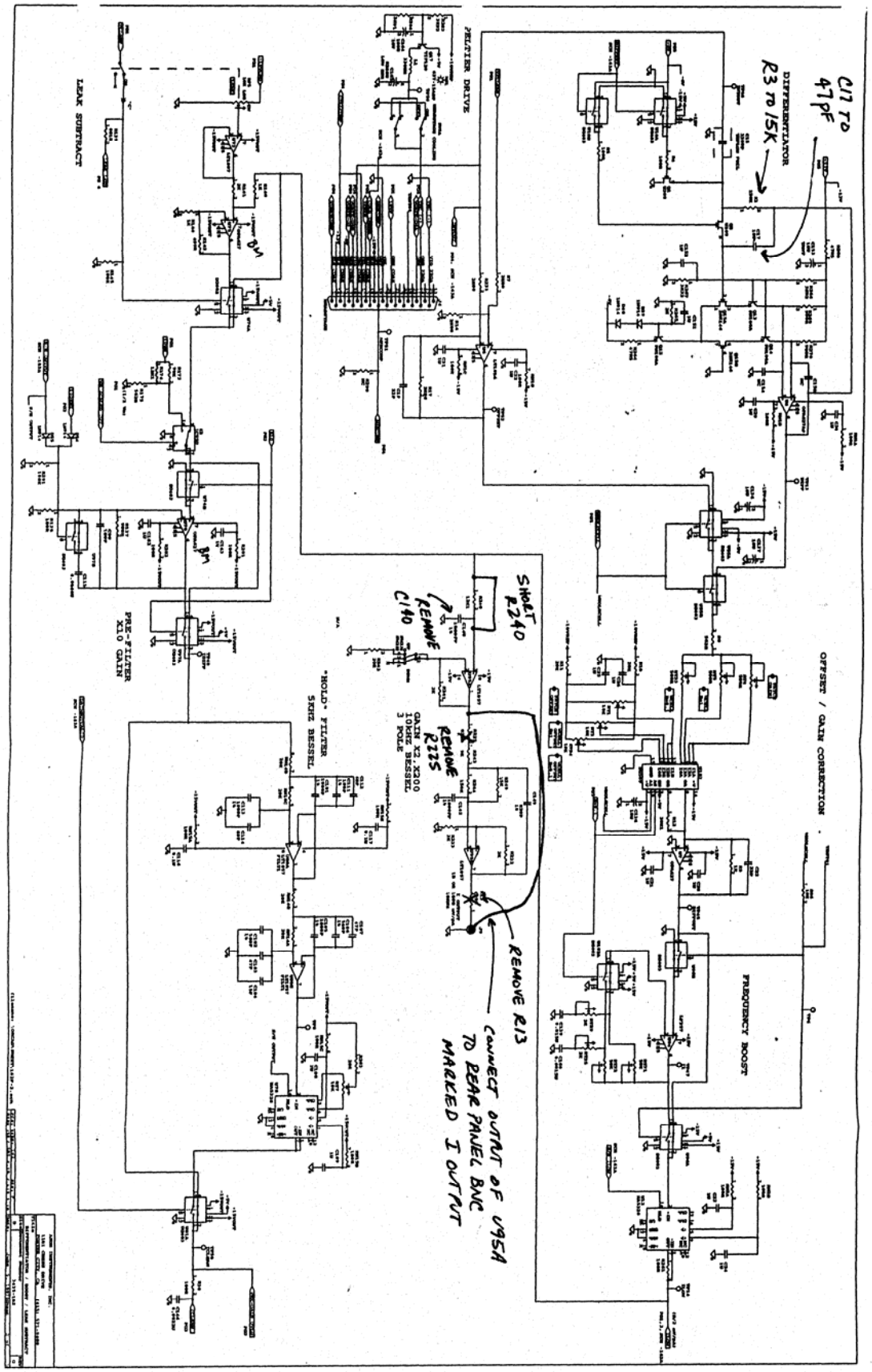

Schema 3.

Diagram of the amplifying circuit of Axopatch 200B and the modifications performed in order to increase the effective bandwidth.

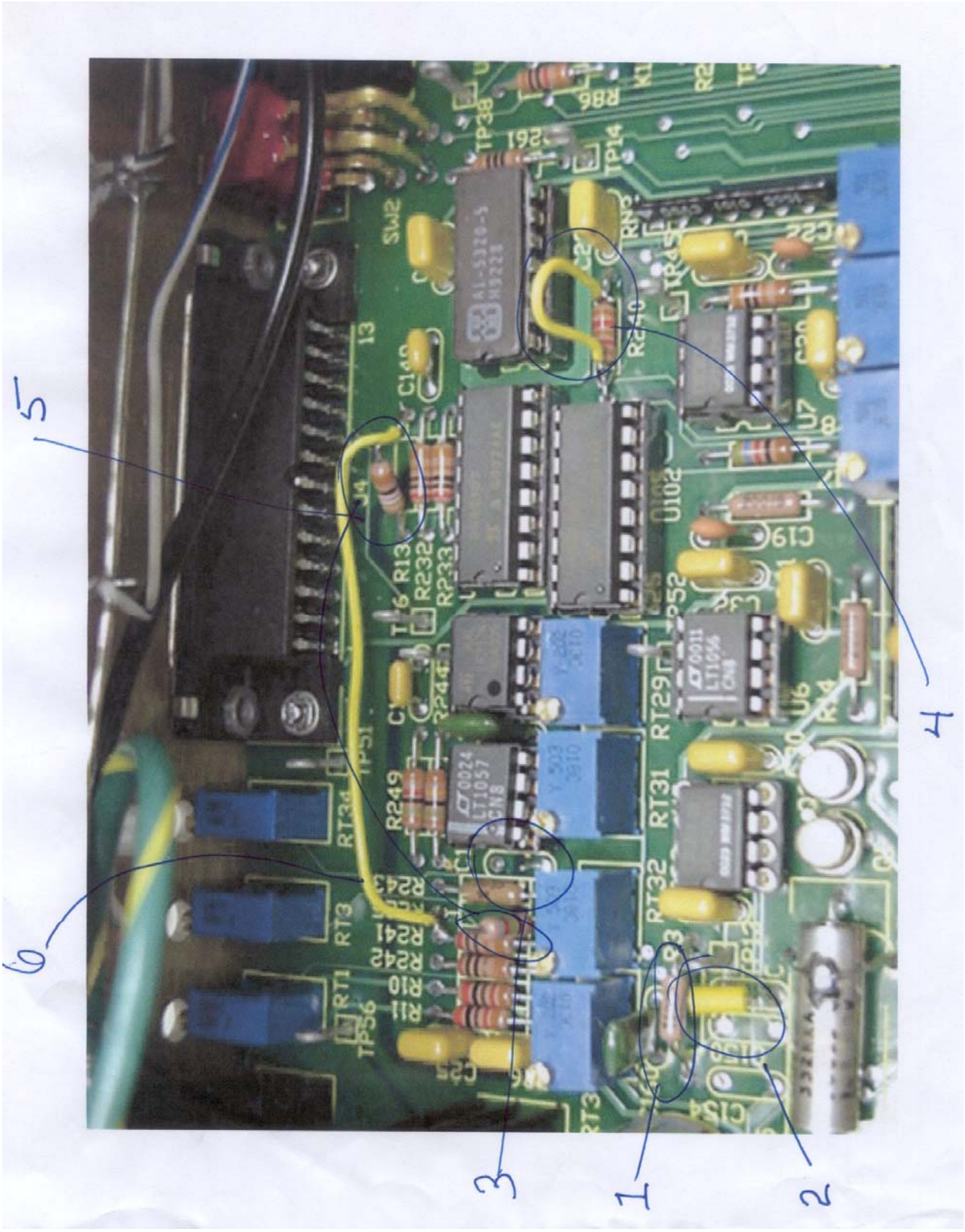

Figure 3. Fragment of the Axopatch 200B circuit board showing the modifications described in Schema 3.

In order to assess the achieved bandwidth, a 10 kHz triangular waveform was capacitively fed into the headstage by bringing an electrode connected to a generator (Exact Electronics, Inc. 124C, Hillsboro OR) near the headstage and pipette assembly. The amplitude of a generated signal and the distance from the electrode to the pipette was adjusted to induce rectangular pulses of current in the headstage with the amplitude corresponding to that of the studied ion channel currents (30 – 120 pA). The generated signal was monitored with an oscilloscope and the transitions between positive and negative slopes of a waveform were verified to take < 0.5 μs. These measurement yielded 10-90% rise time of 2-3 μs, corresponding to the effective bandwidth of ~250 – 300 kHz (Shapovalov and Lester, 2004).

Unprotecting (by bypassing the 10 kHz filer at I_{out}) the output of the U95A amplifier (Schema 3) has rendered the setup sensitive to a significant capacitance of the cable connecting the amplifier to the digitizer and resulted in generation of a high amplitude distortion with frequencies $\geq$ 500 kHz. The 1.5 kΩ resistor introduced in order to protect the amplifier output, removed the distortion but produced additional low-pass filtering of the signal, yielding the effective 10-90% rise time of 2 μs. Fortunately it was possible to find a suitable tradeoff, decreasing this reduction in effective bandwidth by repositioning the amplifier inside the Faraday cage, so that its back output was directly facing the Al wall of the cage and introducing the 4-pole Bessel filter just outside the cage, directly against the amplifier output. A short coaxial cable connection (1 ft.) led from the I_{out} output of the amplifier to the input of the Bessel filter tuned to 2 MHz cutoff frequency to avoid unnecessary bandwidth reduction. This intermediate filtering stage provided adequate protection and alleviated the need for the 1.5 kΩ resistor inhibiting the bandwidth, thus restoring the instrumentation 10-90% response time of 1 μs. On the other hand, a low signal to noise ratio introduced an additional uncertainty, bringing observable 10-90% rise time closer to 2 (after) or 3 (before removal of 1.5 kΩ resistor) μs.

This result sets the limit for the bandwidth achievable by solely tuning the equipment available at

present. Further improvement of the amplifier bandwidth may be possible if the differentiating stage is bypassed completely. Instead, the output signal at operational amplifier A1 on Schema 1B, corresponding to the integral of the current, can be passed directly to the digitizer and the differentiation carried out in software. However such approach imposes very strong requirements on the characteristics of the digitizer employed in the setup. The digitizer needs to provide a dynamic range of 24 bit at 5 MHz or better in order to yield an additional improvement over what can be achieved with the described modifications. Unfortunately such digitizers were not available at the time of this study.

While these modifications drastically reduced apparent rms and peak to peak noise, they did not completely abolish interference from external sources. Figure 4 shows a combination of power spectra generated from traces that measured levels of noise with a headstage in a working position inside a secondary shield both lacking the pipette and with the pipette forming a gigaohm seal on an artificial liposome. Intervals between two consecutive resets of a headstage feedback capacitor (15 sec in a trace from a shielded headstage and 3 sec in a trace from a liposome seal) were chosen for computing power spectra of the signal. It can be seen that at intermediate frequencies (100 Hz to 10 kHz), the thermal noise of the patch is clearly greater than the noise produced by the headstage electronics in a capacitive-feedback mode, whereas at frequencies above 100 kHz both power spectra are similar. This suggests that in order to achieve low levels of noise at bandwidths higher than 100 kHz it is necessary to provide adequate shielding for the instrumentation in the immediate vicinity of the recording chamber. However, at bandwidths below 50 kHz it was critical to keep the stray capacitance as low as possible and the seal resistance as high as possible by employing low-noise techniques, such as the use of quartz pipettes with small tip diameter (Hamill et al., 1981).

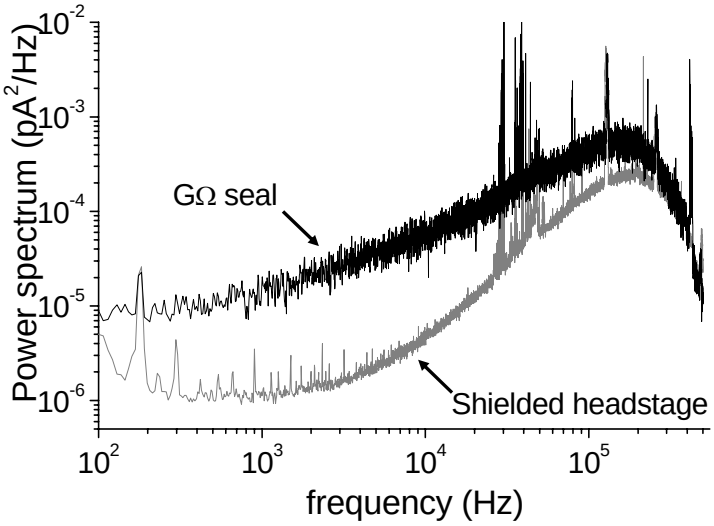

Figure 4. Power spectrum of the noise representing a combination of a baseline noise (smooth curves) and interference (spikes). The gray trace shows noise measured with the headstage near the recording chamber and inside the inner shield, with the pipette holder but without the pipette. The black trace displays the noise measured with the pipette attached and immersed in solution and with a GΩ seal formed.

Collection and analyses of inter-substate transitions

Elementary transition events were collected using a template search routine from Clampfit 9. The template used in the collection procedure was constructed to hold currents at 0 pA and the desired amplitude for 10-20 μs on either side of the transition. To study transitions having smaller amplitude, nearing that of the observed peak to peak noise, additional steps had to be taken to reliably identify transitions, due to low signal-to-noise ratio. Traces recorded at the full bandwidth of ~250 kHz were first subjected to 100 kHz Gaussian digital filter, and the template search routine was then employed to identify downward transitions. Subsequently, 350 μs fragments of original unfiltered traces were extracted starting 50 μs before the onset of the transition for the purpose of dwell time identification. Fragments of 60 μs starting 30 μs before the transition were used for sub-μs alignment as described below. A similar procedure was used to extract MscS substate-2/3 → full conductance transitions.

Individual transitions as well as test pulse responses were fit with $I(t) = A_2 + \frac{A_1 - A_2}{1 + \exp(\frac{t - t_0}{\tau})}$ (a Boltzmann function), where A_1 and A_2 are the amplitudes before and after the transition, t_0 and τ are the transition midpoint, and the slope at midpoint respectively. The slopes at the midpoint were collected and converted to 10-90% transition times ($T_{10\text{-}90} = 2*ln(9)*\tau$). Transition amplitudes were also collected for the analysis of MS ion channel activity.

Analyses described above employed multiple data transformations, such as extracting fragments of the traces and retrospectively realigning them on the x- or y-axis according to set criteria. In order to expedite processing of thousands of collected transitions, the author developed a set of utilities that performed these transformations and could be scripted to automate most of the analyses. The archive containing source of these utilities is available as a supplementary file "analysis_utils.tar.gz" on the Caltech Electronic Theses server at http://etd.caltech.edu/ETD-db/ETD-browse/browse?first_letter=S. The archive contains two major modules. One is "abftools", containing utilities dealing with Axon abf file format and allowing data extraction from and data storage in abf files and related formats. Another one is called "manipulations" and contains higher-level utilities performing tasks such as approximating extracted fragments with Boltzmann or other functions, realigning and averaging fragments, etc. Abftools module is written in C++ and makes use of Axon's abf header structure and the Gnu Scientific Library; higher level utilities in the "manipulations" module are written in Ada-95. A few Python scripts are included as well. The archive can either be compiled in any modern GNU environment with the gcc C/C++ compiler (versions $\geq$3.x) and the gnat Ada compiler (versions $\geq$3.15p) or Ada-enabled gcc (versions $\geq$ 3.5). The executable binaries for local platforms can be built by simply descending to the corresponding module and running make (use "make clean" to remove stale object and executable files) on most UNIX systems or using the Cygwin environment (http://www.cygwin.com) on MS Windows platform.

Bibliography

1993. The Axon Guide for Electrophysiology & Biophysics: Laboratory Techniques.

Benndorf, K. 1995. Low-Noise Recording. *In* Single-Channel Recording. B. Sakmann and E. Neher, editors. Plenum Press, New York. 129-146.

Dudel, J., S. Hallermann, and M. Heckmann. 2000. Quartz glass pipette puller operating with a regulated oxy-hydrogen burner. *Pflugers Arch*. 441:175-180.

Gupta, M.S. 1977. Electrical Noise: Essentials & Sources.

Hamill, O.P., A. Marty, E. Neher, B. Sakmann, and F.J. Sigworth. 1981. Improved patch-clamp techniques for high-resolution current recording from cells and cell-free membrane patches. *Pflugers Arch*. 391:85-100.

Levis, R.A., and J.L. Rae. 1993. The use of quartz patch pipettes for low noise single channel recording. *Biophys J*. 65:1666-1677.

Parzefall, F., R. Wilhelm, M. Heckmann, and J. Dudel. 1998. Single channel currents at six microsecond resolution elicited by acetylcholine in mouse myoballs. *J Physiol*. 512 (Pt 1):181-188.

Shapovalov, G., and H.A. Lester. 2004. Gating transitions in bacterial ion channels measured at 3 micros resolution. *J Gen Physiol*. 124:151-161.